Materials and Design 32 (2011) 1916–1922

Contents lists available at ScienceDirect

Materials and Design

journal homepage: www.elsevier.com/locate/matdes

High-temperature deformation and enhanced ductility of friction stir processed-7010 Aluminum Alloy

Magdy M. El Rayes *[,1], Ehab A. El Danaf, Mahmoud S. Soliman

Mechanical Engineering Department, College of Engineering, King Saud University, P.O. Box 800, 11421 Riyadh, Saudi Arabia

ARTICLE INFO

Article history:
Received 11 August 2010
Accepted 1 December 2010
Available online 5 December 2010

Keywords:
Non-ferrous metals and alloys
Mechanical properties of materials
Plastic behavior

ABSTRACT

In the present study the microstructural and high-temperature mechanical properties of 7010 Aluminum Alloy (AA) resulting from friction stir processing (FSP) were analyzed and compared to unprocessed material. The sheets were processed perpendicularly to the rolling direction that resulted into fine-grained microstructure having the size of about 7 μm. The high-temperature deformation characteristics and mechanical properties of the processed material were studied using hot tensile tests at temperatures of 703, 723 and 753 K and at different strain rates in the range of 1×10^{-2}–1×10^{-4} s^{-1}. Correlation between the flow stress σ and strain rate $\dot{\varepsilon}$ and temperature, T gave an apparent stress exponent n_a of 5 and apparent activation energy Q_a of 260 kJ/mol. The high value of Q_a was attributed to the presence of threshold stress under the present experimental conditions.

1. Introduction

Friction stir processing (FSP) is a new solid state technique which uses the principles of friction stir welding (FSW) to produce materials with fine-grained microstructures as produced by Cavaliere et al. [1]. In FSP, a tool consisting of a shoulder and a concentric pin, which is slightly shorter than the material thickness, is forced into the material being processed until the shoulder comes in contact with its surface. Once the pin has fully penetrated, the tool is allowed to rotate whereas the material linearly moves past the tool. This provides localized frictional heating and mechanical mixing in the area covered by the tool. McNelley et al. [2] have concluded that the severe plastic deformation achieved by the tool stirring action results into large processing strain leading to dynamic recrystallization and consequently microstructural refinement and homogenization. The FSP creates a region called the "stir zone" SZ or "nugget", where the microstructural refinement occurs having an equiaxed-fine grains with high angle grain boundaries. The characteristics of FSP have led to several applications for microstructural modification in metallic materials, including the production of ultrafine-grained (UFG) microstructures amenable to low temperature-high strain rate superplasticity [3–6], dispersing powders into Aluminum matrix to produce high microhardness by the promotion of grain refinement within the nano-scale [7]. Another application of FSP is incorporating nano-sized alumina particles into Aluminum matrix to form particulate composite surface layer [8]. Several researches have succeeded in refining the microstructure of cast Aluminum Alloy such that achieved in the work published [9–11].

Cavalierea and Squillace [12] have studied the high-temperature deformation of FSP-ed 7075 AA using hot tensile tests at different temperatures and different strain rates. This was done in order to analyze the mechanical properties of the recrystallized material and to observe the differences from the parent material as a function of the grain refinement due to the FSP. They found that the strength and ductility of the material increased in the nugget zone with respect to the base material due to the uniform and very fine structure resulting from FSP. In addition, the true stress–true strain response has shown that the flow stress at high temperatures decreases with increasing temperature and also the strain to fracture increases with increasing temperature. However, there is no steady state exhibited by the curves for all the temperatures and strain rates investigated which was in the range of 150–500 °C and 10^{-2}–10^{-4} s^{-1} respectively. It was also reported that the strain rate sensitivity variation obtained at strain = 1 increases upon increasing the strain rate from 10^{-4} to 10^{-3} and then decreases for higher strain rates indicating that FSP-ed material possesses superplastic properties.

The superplastic deformation of FSP-ed 7075 AA has been studied by Ma et al. [13]. In this work two grain size 3.8 and 7.5 μm have been obtained by using different processing parameters. In order to evaluate the microstructural stability the as-processed Aluminum plates were heat treated at 490 °C for 1 h. This treatment revealed that the fine-grained microstructure was stable during hot tensile tests. Superplastic investigations in the temperature range of 420–530 °C and strain rate of 1×10^{-3}–1×10^{-4} s^{-1} demonstrated that a decrease in grain size from 7.5 to 3.8 μm

* Corresponding author. Tel.: +966 1 4679906; fax: +966 1 4676652.
E-mail address: melrayes@ksu.edu.sa (M.M. El Rayes).
[1] On leave from Production Engineering Department, College of Engineering, Alexandria University, Egypt.

0261-3069/$ - see front matter © 2010 Elsevier Ltd. All rights reserved.
doi:10.1016/j.matdes.2010.12.004

resulted in significantly enhanced superplasticity, flow stress, reduced optimum temperature and a shift to a higher optimum strain rate. The analysis of the superplastic data of the two FSP-ed 7075 AA showed that a stress exponent of 2, an inverse grain size dependence of 2 and an activation energy close to that for grain boundary self diffusion. This indicated that grain boundary sliding is the primary superplastic deformation mechanism for FSP-ed 7075 AA.

Furthermore, Mishra and Charit [4] have reported that the combined effect of deformation and temperature leads to very fine grain sizes through the dynamic recrystallization (DRX) process. The probable reason is that a low peak processing temperature and a fast cooling rate kept the post-DRX growth of grains limited. This, in turn, helped in the generation of the UFG microstructure. Furthermore, it was found that with increasing temperature from 230 to 370 °C the flow stress failed down consistently until 410 °C, when an abrupt increase in the flow stress occurred due to abnormal grain growth (AGG). This AGG is characterized by bimodal grain size distribution which is composed of few grains with some form of growth within the fine-grained matrix.

The variation of flow stress as a function of initial strain rate at different temperatures ranging between 220 and 230 °C (presented on double logarithmic scale) has been studied [5]. The slopes of the fitted straight lines corresponding to strain rate sensitivity (m) were 0.33. This value indicates that the deformation model is related to the solute drag dislocation glide mechanism. The concept of this model is that in a certain range of temperatures and applied strain rate, solutes can diffuse to the dislocation cores, saturate them and drag them during dislocation glide. Nevertheless, m values close to 0.5 indicates that grain boundary sliding (GBS) is the dominant deformation mechanism.

The aim of the present work is to study the influence of FSP on microstructural and ductility modifications and to analyze the mechanical behavior of Aluminum Alloy 7010 at different temperatures and strain rates. Special attention will be also paid to elucidate the deformation mechanism of FSP 7010 within the temperature range 703–753 K.

2. Experimental procedure

Commercial 7010 AA plates 3 mm thick, 100 mm wide and 300 mm long with a nominal composition in wt.% 5.7 Zn, 2.4 Mg, 1.84 Cu, 0.29 Si, 0.15 Fe, 0.05 S, 0.03 Mn and the balance is Aluminum were used. A single-pass FSP perpendicular to the direction of elongated grains was carried out at a tool rotational speed of 430 rpm and a traverse speed of 36 mm/min. The tool was manufactured from heat-treated H13 steel with a flat shoulder of 15 mm diameter, and a concentric cylindrical pin with a diameter of 5 mm, and 2.7 mm long. Test set-up which has been used in earlier work [14] is shown schematically in Fig. 1.

Water was used to cool the plate immediately after processing to hinder the growth of the dynamically recrystallized grains. Microstructure characterization was performed using optical microscope (OM). The FSPed specimen was prepared according to the standard procedures for specimen preparation including grinding, polishing and etching. Modified Keller's reagent composed of 2 ml HF (48%), 3 ml HCl (conc.), 20 ml HNO_3 (conc.) and 175 ml distilled water was used to reveal the specimen's microstructure by immersion for 60 s. Grain size was measured by the linear intercept technique. Microhardness measurements were taken on the specimen cross section using Vickers hardness testing instrument at 200 g load and at 0.5 mm distance between successive indentations.

In order to evaluate the mechanical behavior of FSP 7010 Al, miniature tensile specimens (3.0 mm gage length, 2.4 mm gage width and 2.2 mm gage thickness) were wire cut perpendicular to the FSP direction, with the SZ being centered in the gage. These samples were subsequently ground and polished to a final thickness of 2.0 mm. Tensile tests were conducted using an Instron machine model 3385 H, equipped with a computer and a high-temperature split furnace containing three heating zones, at four crosshead speeds corresponding to initial strain rate in the range of 10^{-2}–10^{-4} s^{-1}. Tests were conducted at temperatures of 703, 723 and 753 K in air where the temperature was monitored using a thermocouple connected to the middle of the specimen's gauge section. Load–elongation data were recorded using computer software. Temperatures were monitored using a thermocouple connected to the specimens. After testing, final length of failed specimens was measured to determine ductility.

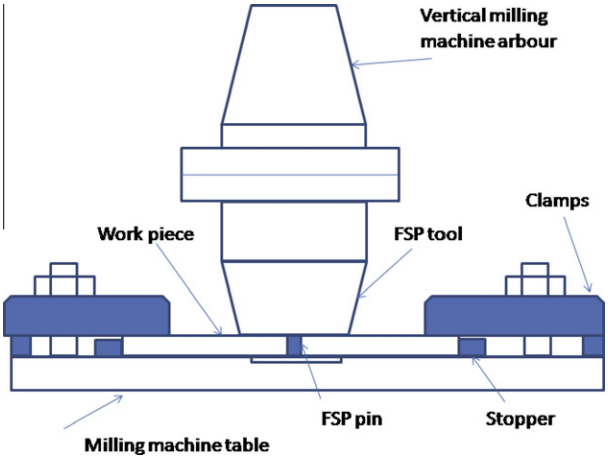

Fig. 1. Experimental set-up for FSP [14].

3. Results

3.1. Microstructural characteristics

Fig. 2a shows an optical microstructure of the base metal, which has large elongated grains, typical to continuously-cast structure. The microstructure of SZ, on the other hand, is characterized by fine and equiaxed recrystallized grains, Fig. 2b. The average grain size in the SZ, determined by the mean linear intercept technique, was within 7–10 μm. The thermo-mechanical affected zone (TMAZ), found in the close vicinity of SZ, is characterized by highly deformed structure, Fig. 2c. In this zone the material experiences lesser strains and strain rates as well as lower peak temperatures compared to the SZ. The TMAZ is often characterized by grain distortion that suggests shearing and flow of material about the rotating tool as found by McNelley et al. [2]. The grain distortion may lead to fragmentation of elongated grains and the formation of refined, equiaxed grains near the interface between the TMAZ and the SZ. The structure in Fig. 2c appears partially recrystallized where some equiaxed grains started to form within the elongated grains. This structure has been found in all the FSP literature related to Aluminum Alloys.

3.2. Hardness test

The microhardness distribution across the processed section is shown in Fig. 3. The microhardness reaches a maximum value of 150 HV at the SZ. Going further from this zone in both the sides at 3 mm far from the center, the hardness value starts to decrease reaching a value around 130 HV at the TMAZ. At about 10 mm from center, corresponding to the unaffected base material, the hardness has stabilized to around 112 HV. The highest hardness at the SZ is

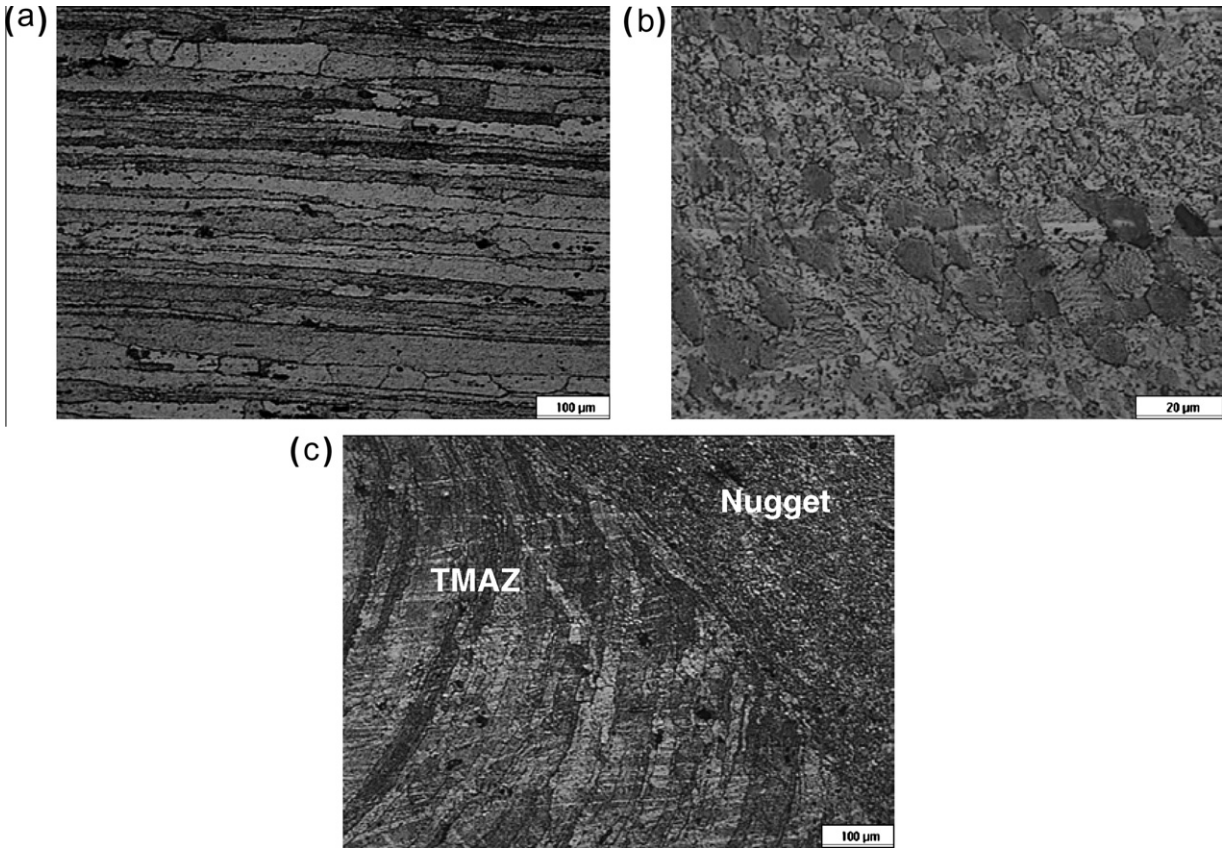

Fig. 2. Optical micrographs showing various zones found in FSP sample: (a) Unaffected base material. (b) Stir zone (nugget). (c) Thermo-mechanically affected zone (TMAZ).

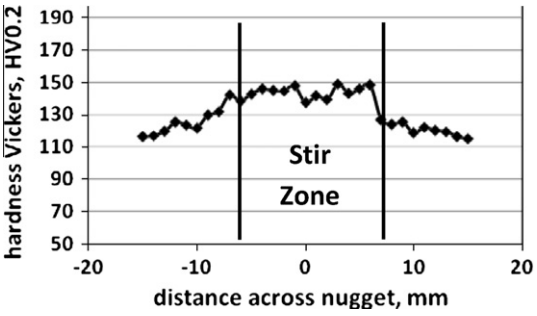

Fig. 3. Microhardness distribution across the FSPed sample.

due to the existence of fine-grained microstructure as well as this zone have experienced severe plastic deformation and consequently strain hardening. The TMAZ is slightly softer than the SZ due to the partial recrystallization as shown in Fig. 2c.

3.3. Stress–strain response

The true stress vs. true plastic strain behavior of FSP specimens for various strain rates at 703, 723 and 753 K are shown in Fig. 4a–c respectively. In general, the flow curves exhibit strain hardening regime, which gets longer when reducing strain rate. At high strain rates; 1×10^{-2} and $2 \times 10^{-3}\,s^{-1}$, the extent of strain beyond the peak stress is relatively limited when compared to lower strain rates; 5×10^{-4} and $1 \times 10^{-4}\,s^{-1}$. The influence of varying the testing temperature can be depicted from the same figure where the flow stress is reduced with increasing temperature at a given strain rate. It can be also noted, that with low strain rates, the flow stress remains nearly constant during the deformation flow, followed by a decrease in flow stress due to necking before failure. The optimum temperature for maximum elongation was found to be 753 K which occurred at a strain rate $1 \times 10^{-4}\,s^{-1}$. Increasing temperature led to a shift of the peak stress to occur at higher strains. Similar trends were found in earlier work [3,6,14].

3.4. Stress dependence of strain rate

The stress dependence of the strain rate under steady state condition at constant temperature is determined by plotting the strain rate, $\dot{\varepsilon}$ as a function of the steady state stress, σ on a double logarithmic scale. Fig. 5 shows this form of plot for three different temperatures 703 K, 723 K and 753 K. Examination of the data of this figure reveals that for the range of strain rates and temperatures tested the data points fall on line segments with stress exponent of 5 and that power law break down is not evident as the curves are linear to high strain rates. The stress dependence of strain rate can be represented by a power function of the form:

$$\dot{\varepsilon} = B\sigma^5 \tag{1}$$

where B is a function of temperature. This behavior could be related to dislocation climb; however, it is necessary to determine the apparent activation energy Q_a to confirm the rate controlling mechanism. This is covered in the next section.

3.5. Apparent activation energy

The apparent activation energy Q_a can be calculated at constant strain rate as

$$Q_a = nR\left[\frac{\partial \ln \sigma}{\partial(1/T)}\right]_{\dot{\varepsilon}} \tag{2}$$

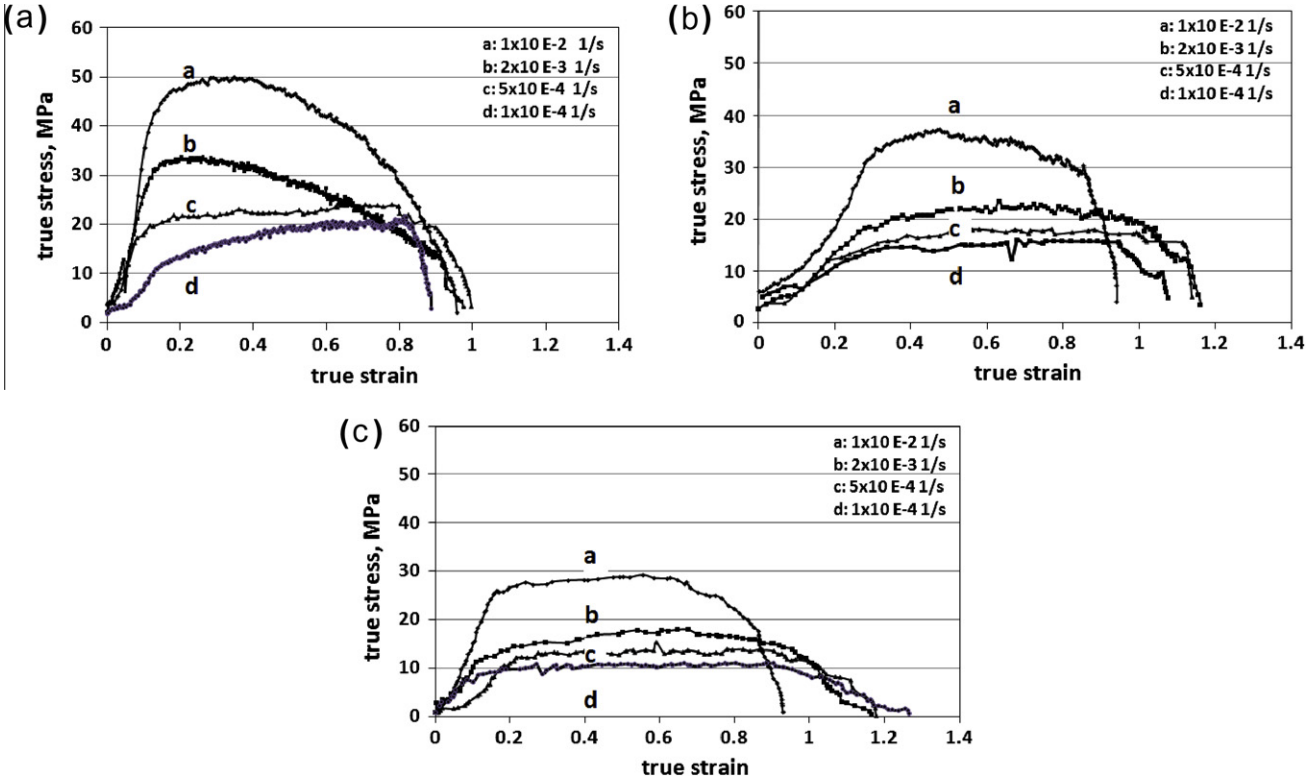

Fig. 4. True stress–true strain curves resulting from hot tensile test of FSPed specimens for various strain rates at different temperatures: (a) 703 K, (b) 723 K, (c) 753 K.

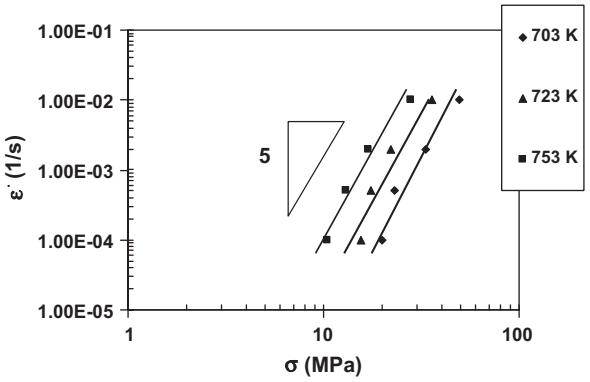

Fig. 5. Double logarithmic scale of stress dependence of strain rate at different temperatures.

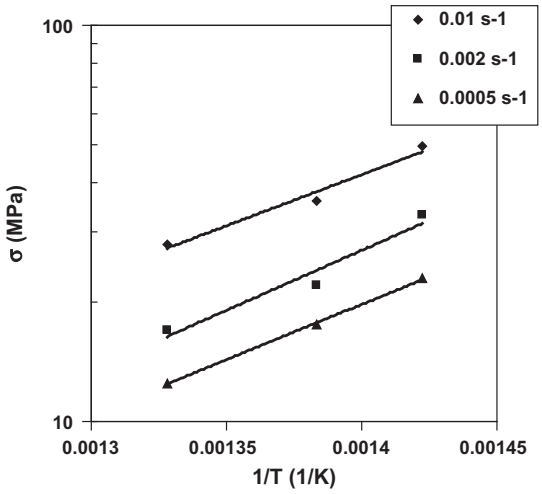

Fig. 6. Semi-logarithmic plot of stress vs. $1/T$ for calculating the apparent activation energy Q_a.

Fig. 6 shows a plot of log σ vs. $(1/T)$. The data points at constant strain rate fall on a segment of straight line whose slope is equal to $\left(\frac{Q_a}{2.3nR}\right)$, which gives Q_a a value of 267 kJ/mol, for the present testing conditions. In calculating Q_a, the value of n was taken as 5, as inferred from Fig. 5. The value of Q_a is much higher than that reported for self diffusion of Aluminum (143 kJ/mol) [15] and Magnesium (130 kJ/mol) [15] alloys. Therefore, high temperature dislocation climb can be ruled out as rate controlling mechanism. This behavior is similar to that reported by Spigarelli et al. [16], for hypereutectic Al–17Si Alloy; $n \sim 5$ and $Q_a = 210$ kJ/mol. This activation energy was substantially larger than that for climb controlled creep.

3.6. Ductility

The variation of elongation; ductility, with initial strain rate at different temperatures is illustrated in Fig. 7. Elongation showed an appreciable dependence on strain rate and temperature especially at 723 and 753 K. At 703 K, however, the variation of elongation with strain rate was limited. A maximum ductility of 254% was obtained at a strain rate of $1 \times 10^{-4}\,s^{-1}$ and 753 K for FSP-ed condition.

Comparing the data of the present work to what has been reported for 7075 AA [13] it was found that strain rate sensitivity m in this work (7010 AA) has a value of 0.2, whereas, with another work applied on 7075 AA it gave a value of 0.5, which infers that the deformation mechanism is mainly carried out by grain boundary sliding. The low strain rate sensitivity obtained in this work has led to lower ductility which could be attributed to the presence of

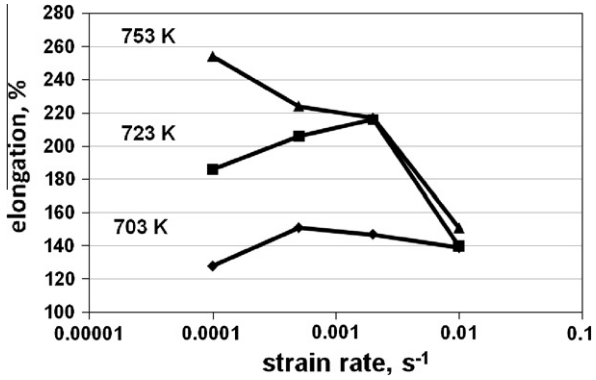

Fig. 7. Variation in elongation with strain rate at different temperatures.

the threshold stress due to the presence of second phase particles which might lead to cavitations thus limiting the total amount of elongation achieved.

3.7. Comparison with the as-received materials at 723 K

As compared with the above-mentioned result, the ductility of the same alloy in the as-received (unprocessed) condition at 723 K is quite low (78%) as reported in the work [17]. Fig. 8 shows the elongations of the present alloy in both the FSP-ed and as-received conditions as a function of strain rate at constant temperature 723 K. Elongation of the as-received material was less

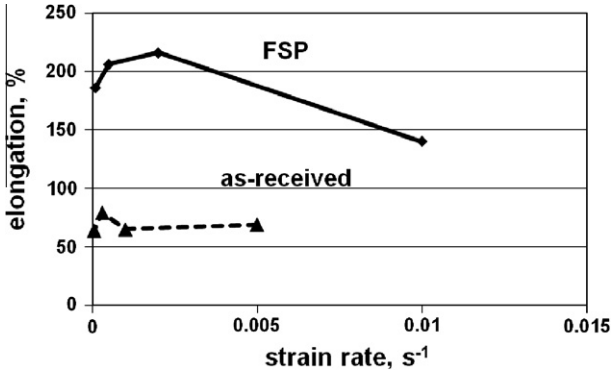

Fig. 8. Comparison between the effect of material conditions on elongation at different strain rates at 723 K.

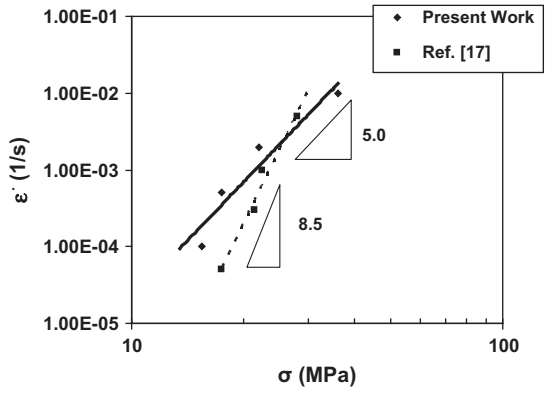

Fig. 9. Stress dependence of the strain rate at 723 K, showing the value of stress exponent for FSP-ed (5) and as-received (8.5) conditions [17].

than 80% and did not exhibit any appreciable dependence on strain rate. On the other hand, FSP-ed AA7010 exhibited a maximum elongation of 217% and demonstrated strain rate and temperature sensitivity with optimum test parameters at 723 K at an initial strain rate of $2 \times 10^{-3}\ s^{-1}$. Fig. 9 shows the stress dependence of strain rate for the two testing condition at 723 K.

4. Discussion

4.1. Threshold stress

The threshold-stress behavior, observed in particle strengthened alloys, can be characterized by two points [15,18]: (i) a high value of stress exponent, n that continuously increases with decreasing stress and (ii) a high value of activation energy above that reported for self diffusion. While the second point is clearly obvious in the results of the present investigation, however, the first point is not. Fig. 5 shows that the value of n is independent of stress and temperature and has a constant value of ≈5. This lack of agreement with point one may be attributed to the limited range of strain rate applied in the present investigation. Under these two conditions, the deformation process is not driven by the applied stress but rather by an effective stress σ_e ($=\sigma - \sigma_o$). Hypereutectic Al–17Si was investigated [16], and found a stress exponent close to 4–5. Although the magnitude of the stress exponent observed was equivalent to that observed in pure Aluminum, the apparent activation energy for creep was higher (Q_a = 210 kJ/mol) than the activation energy for self-diffusion in Al (Q_d = 143 kJ/mol) as reported in previous work [19]. This observation indicated that creep response should be addressed by taking into account more articulated models, they rationalized both the magnitude of the stress exponent and the apparent activation energy for creep, based on threshold-stress concept which arises due to the interaction between fine particles and dislocation. They calculated the true activation energy, taking into account the threshold stress value, to be 160 kJ/mol, which is comparable for that of pure Aluminum. The possibility for the existence of threshold for the present alloy is explored by plotting $\dot{\varepsilon}^{1/n}$ vs. σ, where n was taken 3, using a double linear scale as shown in Fig. 10.

Higher values of n = 5 and 8 were not used because the observed apparent value of n was ~5. This analysis is in good agreement with that reported in the earlier work [16].

The data points for each temperature fall on a segment of straight line with an average correlation factor of 0.99 and the extrapolation of these lines to zero strain rate gives the value of σ_o at each temperature. The values of σ_o are 10, 7.7 and 5.5 MPa at 703, 723 and 753 K, respectively. The present results along with previous studies [15,20–22] suggest that σ_o is a function of temperature and it decreases with increasing temperature. When the

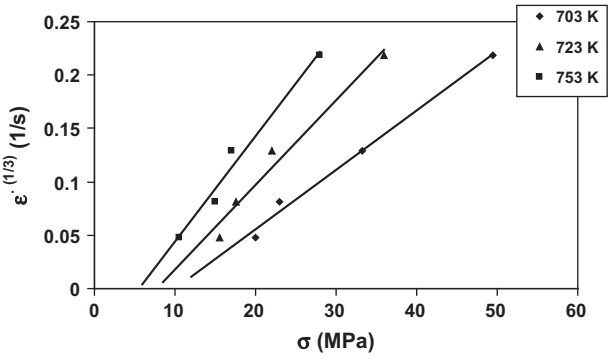

Fig. 10. Double linear plot for $\dot{\varepsilon}^{1/3}$ vs. stress at different temperatures.

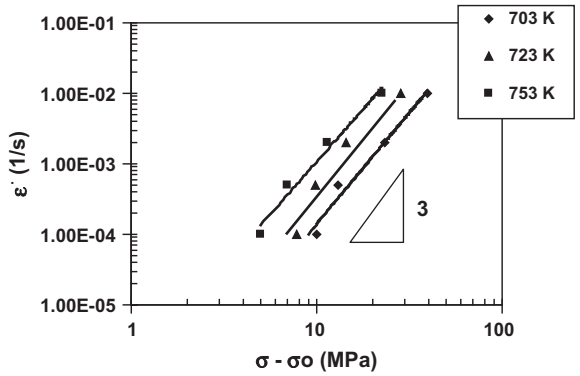

Fig. 11. A double logarithmic plot of strain rate vs. effective stress at various temperatures.

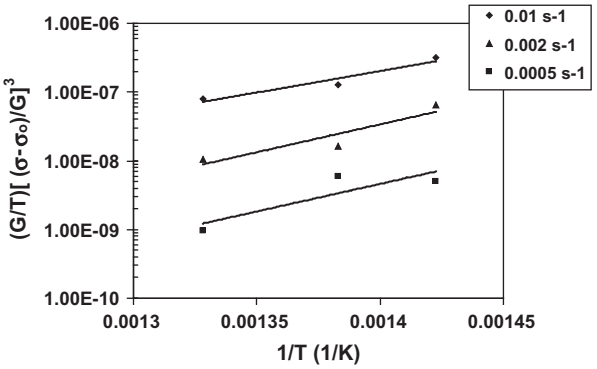

Fig. 12. The relationship between true activation energy Q with $1/T$ at different strain rates.

strain rates are plotted as a function of the effective stress $(\sigma - \sigma_o)$, the data points fall on line segments with an average correlation factor of 0.97 and the stress exponent n inferred is 3 as shown in Fig. 11.

4.2. True activation energy

Under the presence of threshold stress, the Dorn equation can be modified such that the applied stress is replaced by an effective stress. This equation is given by:

$$\frac{\dot{\varepsilon}kT}{DGb} = A_o\left(\frac{\sigma - \sigma_o}{G}\right)^n \tag{3a}$$

with

$$D = D_o \exp\left(\frac{-Q}{RT}\right) \tag{3b}$$

where k is Boltzmann's constant, b is the magnitude of Burgers vector, A_o is a dimensionless constant, Q is the true activation energy for the diffusion process that controls the deformation mechanism and D_o is a frequency factor. Eqs. (3a) and (3b), at constant strain rate, can be rearranged in the form

$$\exp\left(\frac{Q}{RT}\right) = C\left(\frac{G}{T}\right)\left(\frac{\sigma - \sigma_o}{G}\right)^n \tag{4}$$

where C is a constant. Taking the natural logarithm of Eq. (4) and differentiating with respect to $1/T$, the value of Q can be written as

$$Q = R\frac{\partial \ln\left[\frac{G}{T}\left(\frac{\sigma-\sigma_o}{G}\right)^n\right]}{\partial(1/T)} \tag{5}$$

Eq. (5) is used to calculate the true activation energy by plotting $\log\left[\frac{G}{T}\left(\frac{\sigma-\sigma_o}{G}\right)^3\right]$ vs. $1/T$ as shown in Fig. 12. The value of the shear modulus, G (N/m^2) for the alloy as a function of temperature is taken as reported by Iwasaki et al. [23]:

$$G = 4.7859 \times 10^{10} - 1.3571 \times 10^{8}T + 2.6402 \times 10^{5}T^2 - 190.84T^3$$

The value of Q was determined at three various strain rates in the temperature range of 703–753 K. As shown in the figure data points fall on segments of parallel straight lines giving Q a constant value independent of strain rate. The average value of Q was calculated to be 120 kJ/mol. This value is very close to that reported for diffusion of Mg in Aluminum (115–130 kJ/mol) as concluded in the work [24,25].

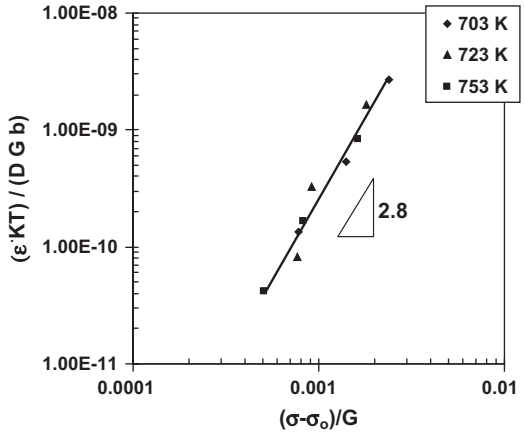

Fig. 13. The constitutive equation expressed in terms of normalized strain rate vs. normalized effective stress.

4.3. Constitutive relation

Using the true activation energy, the normalized creep rate $(\dot{\varepsilon}kT/DGb)$ is plotted vs. the normalized effective stress $(\sigma - \sigma_o)/G$ in Fig. 13. As shown in the figure, the data points coalesce on one segment of straight line with a slope of ~3. A constitutive equation representing the flow characteristics under the present experimental conditions is presented as:

$$\frac{\dot{\varepsilon}kT}{DGb} = 3.86 \times 10^{-2}\left(\frac{\sigma - \sigma_o}{G}\right)^{2.8} \tag{6}$$

This constitutive equation can be used in the finite element analysis of metalworking processes and for evaluating the mechanism of hot deformation either conventionally by using kinetic analysis or more recently by developing processing maps.

5. Conclusions

The main conclusions of this study can be summarized as follows:

(1) Compared to the unprocessed condition of AA 7010, FSP is an effective means for significant ductility enhancement which was obtained when varying the strain rate and temperature.
(2) The deformation behavior of the FSP-AA 7010 Al alloy was examined at temperatures ranging from 703 to 753 K in the strain rate range from 10^{-4} to 10^{-2} s^{-1}. The value of n and Q_a were ≈5 and 267 kJ/mol, respectively.

(3) The calculated true activation energy was independent to strain rate and had a value of 120 kJ/mol, which is close to that reported for diffusion of Mg in Al.
(4) The threshold stress σ_o is a function of temperature where it decreases with increasing temperature, whereas, when plotting the strain rates vs. the effective stress ($\sigma - \sigma_o$), the stress exponent n was 3.
(5) By incorporating the threshold stress into the analysis, a plot of the normalized strain rate, $\dot{\varepsilon}kT/DGb$ vs. normalized effective stress yielded a stress exponent, n of 2.8.

Acknowledgements

The authors would like to express their sincere thanks to the Centre of Excellence for Research in Engineering Materials (CEREM), Faculty of Engineering, King Saud University, in appreciation to its support.

References

[1] Cavaliere P, De Santis A, Panella F, Squillace A. Effect of welding parameters on mechanical and microstructural properties of dissimilar AA6082-AA2024 joints produced by friction stir welding. Mater Des 2009;30:609–16.
[2] McNelley TR, Swaminathan S, Su JQ. Recrystallization mechanisms during friction stir welding/processing of Aluminum alloys. Scr Mater 2008;58:349–54.
[3] Liu FC, Ma ZY. Low-temperature superplasticity of friction stir processed Al–Zn–Mg–Cu alloy. Scr Mater 2008;58:667–70.
[4] Charit I, Mishra RS. Low temperature superplasticity in a friction-stir-processed ultrafine grained Al–Zn–Mg–Sc alloy. Acta Mater 2005;53:4211–23.
[5] Ma ZY, Mishra RS, Mahoney MW. Superplasticity in cast A356 induced via friction stir processing. Scr Mater 2004;50:931–5.
[6] Charit I, Mishra RS. High strain rate superplasticity in a commercial 2024 Al alloy via friction stir processing. Mater Sci Eng A 2003;359:290–6.
[7] Morisada Y, Fujii H, Nagaoka T, Nogi K, Fukusumi M. Fullerene/A5083 composites fabricated by material flow during friction stir processing. Composites Part A 2007;38:2097–101.
[8] Shafiei-Zarghani A, Kashani-Bozorg SF, Zarei-Hanzaki A. Microstructures and mechanical properties of Al/Al_2O_3 surface nano-composite layer produced by friction stir processing. Mater Sci Eng A 2009;500:84–91.
[9] Ma ZY, Sharma SR, Mishra RS. Effect of friction stir processing on the microstructure of cast A356 Aluminum. Mater Sci Eng A 2006;433:269–78.
[10] Ma ZY, Pilchak AL, Juhasb MC, Williams JC. Microstructural refinement and property enhancement of cast light alloys via friction stir processing. Scr Mater 2008;58:361–6.
[11] Santella ML, Engstrom T, Storjohann D, Pa T-Y. Effects of friction stir processing on mechanical properties of the cast Aluminum alloys A319 and A356. Scr Mater 2005;53:201–6.
[12] Cavalierea P, Squillace A. High temperature deformation of friction stir processed 7075 Aluminum alloy. Mater Charact 2005;55:136–42.
[13] Ma Z, Mishra RS, Mahoney MW. Superplastic deformation behavior of friction stir processed 7075 Al alloy. Acta Mater 2002;50:4410–30.
[14] El-Danaf EA, EL-Rayes M, Soliman MS. Friction stir processing: an effective technique to refine grain structure and enhance ductility. Mater Des 2010;31:1231–6.
[15] Mohamed FA. Correlation between creep behavior in Al-based solid solution alloys and powder metallurgy Al alloys. Mater Sci Eng A 1998;245:242–56.
[16] Spigarelli S, Evangelista E, Cucchieri S. Analysis of creep response of an Al–17 Si–4 Cu–0.55 Mg alloy. Mater Sci Eng A 2004;387–389:702–5.
[17] Almajid AA. High temperature deformation of solution treated 7010 Aluminum alloy. J King Saud Univ Eng Sci, in press.
[18] Evangelista E, Spigarelli S. Constitutive equations for creep and plasticity of Aluminum alloys produced by powder metallurgy and Aluminum based metal matrix composites. Metall Mater Trans A 2002;33A:373–81.
[19] Kassner ME, Perez-Prado MT. Five power-law creep in single phase metals. Prog Mater Sci 2000;45:1–102.
[20] Kaibyshev R, Sitdikov O, Mazurina I, Lesuer DR. Deformation behavior of a 2219 Al alloy. Mater Sci Eng A 2002;334:104–13. doi:10.1016/S0921-5093(01)01777-4.
[21] Marquis EA, Seidman DN, Dunand DC. Effect of Mg addition on the creep and yield behavior of an Al–Sc alloy. Acta Mater 2003;51:4751. doi:10.1016/S1359-6454(03)00288-.
[22] Kaibyshev R, Musin F, Avtokratova E, Motohashi Y. Deformation behavior of a modified 5083 Aluminum alloy. Mater Sci Eng A 2005;392:373.
[23] Iwasaki H, Hosokawa H, Mori T, Tagata T. Quantitative assessment of superplastic deformation behavior in a commercial 5083 alloy. Mater Sci Eng A 1998;252:199–202.
[24] Hirano K, Fujikawa S. Diffusion of 28 Mg in Aluminum. J Nucl Mater 1978;69–70:564–70.
[25] Rothman SJ, Peterson NL, Nowicki LJ, Robinson LC. Tracer diffusion of Magnesium in Aluminum single crystals. Phys Status Solidi B 1974;63:K29–33.